UPPSALA
UNIVERSITET

UPTEC Q 20012
Examensarbete 30 hp
Oktober 2020

Magnetron sputtering of highly transparent p-conductive NiO thin films

Martin Book

UPPSALA
UNIVERSITET

Teknisk- naturvetenskaplig fakultet
UTH-enheten

Besöksadress:
Ångströmlaboratoriet
Lägerhyddsvägen 1
Hus 4, Plan 0

Postadress:
Box 536
751 21 Uppsala

Telefon:
018 – 471 30 03

Telefax:
018 – 471 30 00

Hemsida:
http://www.teknat.uu.se/student

Abstract

Magnetron sputtering of highly transparent p-conductive NiO thin films

Martin Book

P-type transparent conductors are needed for a wide range of applications such as solar cells and electrochromic smart windows. Solar power is an important form of energy in today's society as the threat of global warming pushes the world towards fossil free energy. Hence a lot of solar cell types have been developed, among them tandem cells which are two different types of solar cells stacked on top of each other. If one of the cells is based on a perovskite, a transparent p-type thin film electrode is needed as a hole conductor and electron blocking layer between the two cells. Nickel oxide (NiO) is a good candidate for this application as it has desired properties such as good hole conduction, a high band gap and a matching work function to the perovskite. The transmittance of as deposited NiO films by reactive magnetron sputtering is limited so post deposition annealing is used to increase the transmittance. This is not possible in this solar cell application as parts of the solar cell stack is temperature sensitive.
Electrochromic smart windows contain a layer that can change its optical properties with the application of a voltage. Such windows are used in buildings to increase energy efficiency and they contain an electrochromic device where NiO is used as an electrode as it has electrochromic properties, but just like with the solar cells, the transmittance of NiO is limited. This study investigates whether it is possible to make as deposited NiO by reactive magnetron sputtering transparent, eliminating the need for post deposition annealing. Such a deposition process was found using different sputter machines with the process point on the edge between metal and oxide mode in terms of oxygen flow. This resulted in highly transparent and highly resistive NiO films with a much higher deposition rate than in oxide mode.

Handledare: Tomas Kubart
Ämnesgranskare: Tobias Törndahl
Examinator: Åsa Kassman Rudolphi
ISSN: 1401-5773, UPTEC Q20012

Magnetronsputtring av transparenta och p-ledande tunnfilmer av NiO

Martin Book

Behovet av transparenta p-ledande material ökar ständigt i och med att marknaden för tillämpningarna ständigt växer. Dessa inkluderar bland annat solceller och så kallade smarta fönster. Det ständiga hotet från global uppvärmning leder till att forskningen kring fossilfria energislag ökar, däribland solceller. En speciell typ av solcell kallas tandemsolcell vilken i sin helhet är två solceller ovanpå varandra. Tanken är att det ljus som inte absorberas i det övre lagret ska absorberas i det undre vilket ökar effektiviteten genom att en större del av solljuset absorberas. I skiktet mellan de två cellerna krävs transparenta elektroder, varav en av p-typ, för att släppa igenom så mycket ljus som möjligt och för att underlätta transport av laddningsbärare. Om en av cellerna är baserad på perovskiter är Nickeloxid (NiO) en bra kandidat som p-ledande och elektronblockerande elektrod. Nickeloxid har önskvärda egenskaper, bland annat bra ledning av hål, ett högt bandgap vilket gör att alla synliga våglängder släpps igenom, samt en utträdesfunktion som matchar den hos perovskiten vilket ökar effektiviteten hos cellen. Det finns däremot en viss ljusabsorption i hela det synliga spektrat för magnetronsputtrad NiO. Denna kan minskas med värmebehandlingar men då delar av solcellen är temperaturkänslig är detta inte möjligt i denna tillämpning.

En typ av smarta fönster är elektrokroma fönster som reversibelt kan ändra sina optiska egenskaper genom att en spänning appliceras. Sådana fönster är lämpliga på fasader vilket kan göra byggnaderna mer energieffektiva då mindre el går åt till att kyla dem. I den elektrokroma delen av fönstret används NiO som elektrod. Materialet har elektrokroma egenskaper men samma problem som för solcellen finns här, nämligen att det finns en viss ljusabsorption.

Målsättningen med detta projekt har varit att utforska huruvida det är möjligt att tillverka en transparent tunnfilm av NiO med reaktiv magnetronsputtring, vilket skulle eliminera behovet av värmebehandling och således öka effektiviteten hos solcellen och minska absorptionen i de smarta fönstrerna. Stuidien visar att en sådan tunnfilm kan tillverkas genom att låta syreflödet i tillverkningen ligga väldigt nära gränsen för metall och oxidläge. Processen bekräftades genom att uppnå liknande resultat i olika sputtermaskiner. Den deponeringsprocess som tagits fram gör det möjligt att deponera tunnfilmer som ligger väldigt nära värmebehandlade filmer när det gäller absorption. De resulterande filmerna är även väldigt resistiva, vilket visar att processen ger en NiO som är väldigt nära stökiometrisk. Tillväxthastigheten som uppmättes var högre än i metalläge och 5-7 gånger högre än i oxidläge trots att det är samma material som deponerats.

Examensarbete 30 hp på civilingenjörsprogrammet
Teknisk fysik med materialvetenskap
Uppsala universitet, Oktober 2020

Contents

1 Introduction

1.1 Project outline

This diploma project investigates deposition of transparent nickel oxide (NiO) films using reactive magnetron sputtering. The aim was to develop a deposition process that produces highly transparent films without the need for post deposition annealing. In the course of the project, the influence of the deposition parameters on the optical and electrical properties of the films was studied. In order to verify the findings, two different sputter deposition systems were used and the results were compared. The films were examined using spectrophotometry, scanning electron microscopy (SEM) and sheet resistance measurements.

The work is of importance for various applications where NiO is used. This includes solar cells where NiO acts as an electron blocking layer. For instance, tandem solar cells with CIGS bottom and perovskite top cells as the electron blocking layer in the middle of the tandem stack. The existing NiO has low transmittance which results in optical losses. Post deposition annealing could not be used due to the temperature sensitivity of the CIGS. The new deposition process is therefore interesting.

The newly developed NiO is also relevant as an electrode in electrochromic windows. Here, high transmittance is also important. Therefore, the new process is also evaluated in this area.

1.2 Sputtering

Sputtering is a technique used for thin film deposition from a solid material. Atoms of the source material, sputtering target, are ejected by bombardment with energetic ions, usually argon ions. The source of these ions is a plasma created by applying a high negative voltage to the target, a glow discharge. The ions from the plasma are then accelerated towards the target with enough energy to eject atoms from the target and initiate sputtering [1, 2]. The glow discharge can be excited in several ways, namely by direct current (DC), radio frequency (RF), or medium frequency (MF) power.

In order to increase the amount of ions and to sustain the plasma, a magnetic field can be formed in front of the target. This magnetic field traps electrons, confining the plasma to the target, allowing a higher production of ions at the same electron density which in turn leads to a higher deposition rate. This is called magnetron sputtering [2]. The magnetron can be powered with either direct current or alternating current (AC). AC sputtering is usually done at a frequency of 13.56 MHz which is in the radio region and hence it is often called radio frequency sputtering. One drawback to using magnetron sputtering is nonuniform target erosion leading to poor utilization of the target [2].

When using reactive magnetron sputtering, a reactive gas is introduced to the sputtering chamber, for instance oxygen when depositing an oxide. The sputtered atoms then undergo a chemical reaction with the gas before hitting the substrate. [1, 2] There are some challenges in reactive sputtering, mainly that

the target also will get oxidized and since most of the compounds produced with reactive sputtering are electrical insulators, charge build up on the target can occur. This can lead to an arc discharge which results in particle ejection. These particles, macroparticles, can be incorporated into the films with detrimental impact on the film quality [2, 3]. In the case of RF sputtering this is not a problem as the oscillation of the current reaches a positive voltage with every cycle, discharging the target. A DC offset is used to tune the length of the sputtering and discharge in each cycle [2]. The way to prevent this arc discharge in DC sputtering is to neutralize the surface charge. This is used in so-called pulsed DC sputtering. What happens here is that the voltage is periodically changed to a positive one to discharge the target. This essentially mimics a square AC wave [3]. Another thing to be aware of with reactive sputtering is hysteresis effects due to changes in the flow of the reactive gas [2]. The hysteresis effect can clearly be seen in figure 1.

Using DC to sputter a non conductive material is impossible as the resistivity of the target will be too high to pass a current and the plasma will be extinguished. To sputter non conductive materials, RF sputtering has to be used. The non conductive target can be seen as a dielectric in a capacitor and the impedance of capacitor is inversely proportional to the AC frequency. Due to the high frequency used in RF sputtering, this allows a current to pass through the non conductive target making it possible to sputter [1].

Sputtering of a ferromagnetic material using DC sputtering can be tricky since the magnetic field that usually confines the plasma to the target, does not penetrate the target material. [4] There are however ways to get by this problem. Using very strong magnets and a thin target can allow the material to be saturated and hence allow magnetic flux to penetrate it [4].

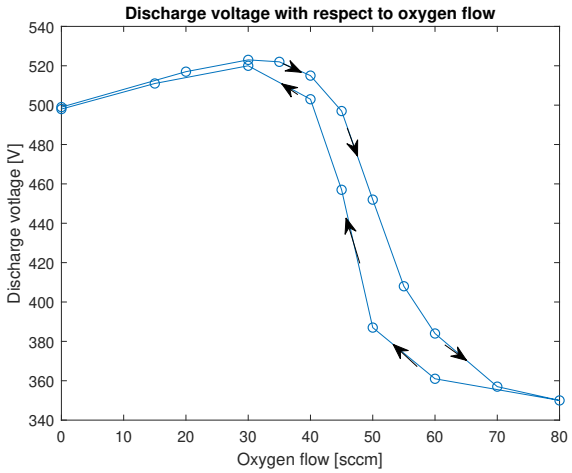

Figure 1: Discharge voltage as a function of oxygen flow for the low pressure depositions done in the FHR roll to roll sputter. The hysteresis can clearly be seen. Equally abrupt change can be observed in the oxygen partial pressure or deposition rate.

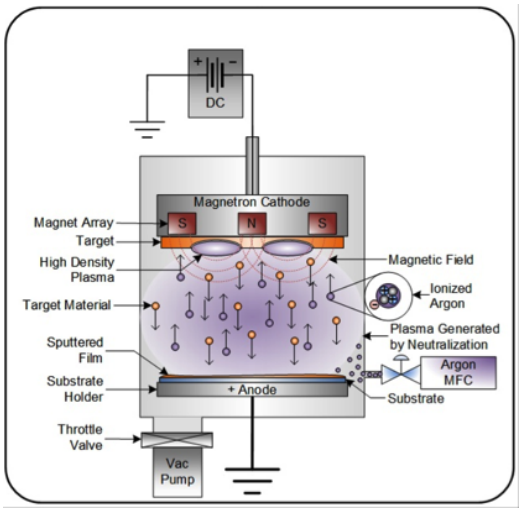

Figure 2: Illustration of a DC magnetron sputtering system. An RF sputtering system is very similar with the main difference being the power supply. Source: Matt Hughes [5].

1.3 Applications for sputtered nickel oxide

NiO is a p-type transparent conductor. As such, it can be used in many areas. There are two areas where sputtered NiO is used that have been investigated in this project. In solar cells it is used as an electron blocking layer and in smart windows it is used as an electrode. In both cases a high transmittance is desired.

1.3.1 Solar cells

In recent years, research on perovskite based solar cells has been on the rise. The most common perovskite used, methylammonium lead iodide ($CH_3NH_3PbI_3$), has a direct optical band gap at 1.5 eV which covers the visible spectrum [6]. This material is also intended for use in so called tandem solar cells where two solar cells are stacked on top of each other. It is important to have both good n-type and p-type contact materials for such a device, however finding a good p-type material has proven to be difficult and to date none have been found that can match the performance of the n-type materials in use today [7]. NiO is a good p-type candidate intended for use as an electron blocking, hole conducting electrode between the stacks. This is because it has some properties that are ideal for use in such solar cells namely that it is a good hole conductor, is chemically stable and has a work function that can be tuned within the interval 5.0 to 5.6 eV. This aligns with the work function of the perovskite which is at 5.4 eV decreasing losses during charge transfer which increases efficiency [6]. The optical transmittance can be an issue as some of the light will be lost and hence a high transmittance is required in order for the light to reach the bottom cell. Earlier tests at Ångström resulted in about 20% optical losses in as deposited NiO.

1.3.2 Smart windows

One type of smart window utilizes something called electrochromism. A material that is electrochromic is able to reversibly change its optical properties by the application of a voltage [8]. There are several applications for electrochromic devices but the main use today is in windows for buildings to make them more energy efficient as they might lessen the need for air conditioning [8, 9].

A basic electrochromic device consists of five layers in or in between two substrates, in this case glass. As can be seen in figure 3 the layers are a transparent conductor, an electrochromic film, an electrolyte, an ion storage layer or another electrochromic film and finally another transparent conductor. If two electrochromic layers are used, it is important that they are not made of the same material as one has to conduct ions and the other needs to be able to store them [8]. When a voltage is placed over the two transparent conductors, ions are transferred from the ion storage film through the electrolyte to the electrochromic film which alters the optical absorption of it. Reversing the voltage will cause the electrochromic films to revert to their original state [8]. NiO has electrochromic properties and in the type of electrochromic device described it is used as the ion storing electrochromic film with the other electrochromic film usually being made of tungsten oxide. [8]. A problem with NiO is an unwanted relatively high absorption in the middle of the visible spectra. This however can be mitigated by adding aluminium or manganese to the NiO [9]. In contrast to the solar cells, a certain porosity is required here to facilitate the ion transfer, increasing the electrochromic activity [10].

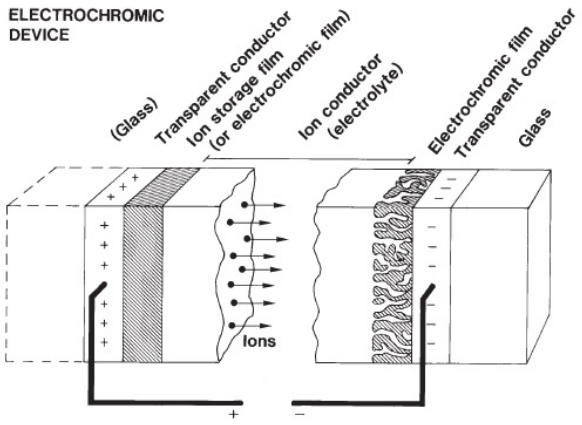

Figure 3: A basic electrochromic device with its different parts. Source: Gunnar A Niklasson and Claes G Granqvist [8].

2 Theory

2.1 Properties of nickel oxide

2.1.1 Bulk properties

Stoichiometric NiO is an insulating metal oxide that crystalizes in the rock salt (NaCl) structure. NiO has a lattice parameter of 4.173 Å and a density of 6.67 g/cm^3. The band gap is around 4 eV which leads to strong absorption in UV and the refractive index is 2.33 [10]. Pure NiO has an absorption coefficient between $5 \cdot 10^2$ - 10^3 cm^{-1} in the visible region [11]. It is considered not to be possible to make stoichiometric NiO as it will always be nickel deficient and hence there will be an excess of oxygen in the structure although annealed NiO seems to be close to being stoichiometric [10, 12]. The extra oxygen atoms can not be interstitially placed in the crystal which leads to nickel vacancies being formed. These vacancies lead to some Ni^{2+} ions being converted to Ni^{3+} to preserve charge neutrality. It is these Ni^{3+} ions that give rise to a p-type conduction in the material [12, 13]. Apart from vacancies, other defects such as impurities will likely be present [10]. Dopants can also be used to alter the conductivity [12].

2.1.2 Thin film properties

Thin films of NiO deposited by magnetron sputtering are grey in color with some transmittance and fairly low resistivity [14]. The transmittance depends on the sputtering system as well as the parameters used during the deposition. It is well known that annealing the NiO makes it more transparent and resistive [14]. When annealing, oxygen seems to diffuse out reducing the amount of Ni^{3+} ions and thereby the amount of defects in the structure that can absorb and scatter light making the films more transparent [13]. Fewer Ni^{3+} ions also lead to an increase in resistivity as they are the source for the conductivity. [15, 16]. There is however, a possibility that sputtered NiO can be made somewhat transparent without annealing resulting in a semi-oxidized film [16, 17].

There are four main thin film properties that are of interest in this report, sheet resistance as well as the transmittance, reflectance and the absorption coefficient. They will be explained in this section.

2.2 Sheet resistance

To electrically characterize a sample, the resistance is most often used. The resistance however is a bulk property and is not all that suitable to use when characterizing a thin film as it cannot be measured directly. Instead it is more common to use the sheet resistance to characterize such samples. The sheet resistance is a measurement of the lateral resistance through a thin sample and it is useful since it is independent of the sample size making comparisons between samples of different sizes easy, unlike resistance which is dependent on dimensions of the sample. It is defined as the resistivity, ρ divided by the thickness, t as can be seen in equation 1. The unit is Ω but $\Omega/\square$ is more commonly used to avoid

confusion with the bulk resistance [18, 19].

$$R_s = \frac{\rho}{t} \tag{1}$$

There are several ways to measure the sheet resistance with the most common method being the four-point probe method. This setup consists of four probes in the corners of a square or in a line with equal spacing. In the linear type, a current is then placed between the two outer probes and the voltage drop is then measured between the two inner pins. The advantage of using this configuration is that the contact resistance does not effect the measurement. The sheet resistance can then be calculated using the following equation (2) [18, 20]:

$$R_s = \frac{V}{I} \cdot \frac{\pi}{ln2} \tag{2}$$

2.3 Transmittance, reflectance and absorption coefficient

There are three basic properties of a solid material when interacting with light, reflection, propagation and transmission. When a beam of light hits the surface of a material, some of the light will be reflected back from the surface while the rest will begin to propagate through it. If all the light that enters the material and propagates through it reaches the other end of the material it can be reflected again or it will be transmitted. There are several absorption mechanisms for light in a solid material and all absorption happens while propagating through the material. The light that is not absorbed will be transmitted [21]. The amount of incident reflected, absorbed and transmitted is equal to the total amount of incident light. These quantities are dependent on the wavelength of the incident light which gives the following relation (3):

$$R(\lambda) + T(\lambda) + A(\lambda) = 1 \tag{3}$$

To quantify the absorption through a medium the absorption coefficient, α, can be used. It is defined as the fraction of the incident light that is absorbed in a unit length. This makes it useful since it is independent of the thickness of the material. Using equation 4, called Beer's law, the absorption coefficient, can be extracted which gives equation 5 [21].

$$I = I_0 e^{-\alpha z} \tag{4}$$

$$\alpha = (\frac{1}{z}) ln[\frac{I}{I_0}] \cdot \tag{5}$$

Where I is the intensity of transmitted light, I_0 is the intensity of the incident light and z the distance the light has travelled.

2.4 Scanning electron microcope

SEM is a powerful microscopy tool where electrons are used rather than light as the lower wavelength of electrons allows for a much larger magnification. This however, means that the sample has to be electrically conductive to allow the removal of excess electrons preventing charge build-up which otherwise causes distortions in the acquired image as the incoming electrons will be deflected. This problem is usually circumvented by coating the substrate with a thin conducting film by either evaporation or sputtering [22]. Other methods include using a conductive tape to increase the electrical contact between the sample and the sample holder.

3 Experimental

3.1 Deposition

Depositions were done at Ångström using two different laboratory size sputtering systems and at a company using a roll to roll industrial sputter.

3.1.1 Ångström

The depositions of the NiO was done on soda-lime glass with reactive magnetron sputtering. Two different sputtering devices were used for the depositions, a Kurt J. Lesker CMS-18 and a Von Ardenne CS 730S. For the initial set of depositions the only thing which varied in the Von Ardenne sputter was the oxygen flow. In the Lesker the deposition time was varied to get a thick enough film to make comparisons with the Von Ardenne samples. Due to nickel being a magnetic element, RF-sputtering was used in the Lesker sputter while the design of the target in the Von Ardenne allowed the use of pulsed DC-sputtering.

The following parameters were used for the first set of depositions in the Von Ardenne and Lesker.

Table 1: Table of sputtering parameters used in the Von Ardenne sputter.

Parameter	
Target	Nickel
Target diameter	6"
Sputtering power	500 W
Sputtering mode	Pulsed DC
Target-substrate distance	55 mm
Chamber pressure	$6 \cdot 10^{-3}$ torr
Deposition time	120 s
Ar flow	25 sccm
O_2 flow	0-50 sccm

Table 2: Table of sputtering parameters used in the Lesker sputter.

Parameter	
Target	Nickel
Target diameter	4"
Sputtering power	250 W
Sputtering mode	RF
Target-substrate distance	180 mm
Chamber pressure	$1 \cdot 10^{-3}$ torr
Deposition time	600-3600 s
Ar flow	50 sccm
O_2 flow	0-5 sccm

The second set of depositions only utilized the Von Ardenne sputter, investigating whether a transparent NiO could be deposited if the depositions were done close to the edge between metal and oxide mode in the reactive sputtering process. The same parameters were used apart from the O_2 flow which was varied in a much more narrow range. A total of four depositions were done here with an O_2 flow of 6, 7, 8 and 9 sccm respectively. A 0.8 cm $\cdot$ 0.8 cm oxidized silicon substrate was deposited on at the same time for use in Hall and XPS measurements.

Subsequent depositions were made to verify reproduciblity of the results from the second set. Quartz was used as a substrate for these depositions. The quartz samples were used in order to evaluate possible differences in the band gap of the NiO depending the oxygen flow used. Pieces of oxidized silicon were put in the deposition chamber during these depositions as well.

The Lesker sputter was once again utilized for the final set of depositions due to its mass flow controller allowing for smaller increments in the oxygen flow making it easier to deposit films in and around the transition region.

3.1.2 Industrial sputter

Some depositions were done on an FHR RC 200-3 sputter which uses a roll to roll process and DC-magnetron sputtering. The sputter used can be seen in figure 4 and 5. These depositions were done on a polymer foil which passed through the deposition chamber at a speed of 0.1 m/min. Two sets of depositions were done with two different chamber pressures which was regulated by the argon flow. Before these depositions were done, a rough estimate of the transition region would be was investigated by changing the oxygen flow and observing the discharge voltage. The oxygen flows in both cases were chosen based on observed discharge voltages. The depositions were done at an oxygen flow that should be right before or at the beginning of the transition region and the oxygen flow was subsequently increased every five minutes to give a 0.5 meter sample at each flow. The depositions ended when a flow close to the oxide edge of the transition was reached. The first and last 15 cm of each sample part were discarded to ensure that the remaining 20 cm would be unaffected by the previous or next oxygen flow region of the foil.

The following sputtering parameters were used in the roll to roll depositions (Table 3 and 4).

Table 3: Table of sputtering parameters used in the roll to roll sputter with low pressure.

Parameter	
Target	Nickel
Sputtering power	2000 W
Sputtering mode	DC
Chamber pressure	$8 \cdot 10^{-3}$ torr
Roll speed	0.1 m/min
Ar flow	75 sccm
O_2 flow	30-65 sccm

Table 4: Table of sputtering parameters used in the roll to roll sputter with high pressure.

Parameter	
Target	Nickel
Sputtering power	2000 W
Sputtering mode	DC
Chamber pressure	$20 \cdot 10^{-3}$ torr
Roll speed	0.1 m/min
Ar flow	225 sccm
O_2 flow	40-80 sccm

Figure 4: The FHR sputter used for the roll to roll depositions.

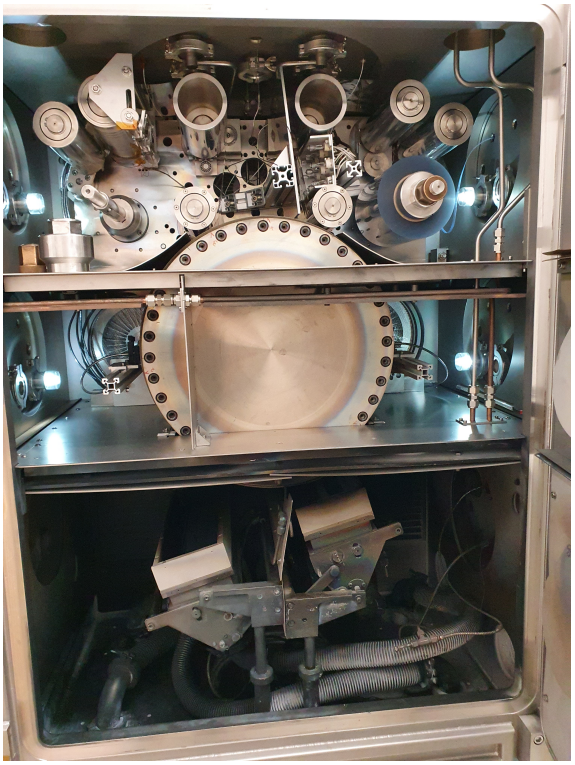

Figure 5: Inside the FHR sputter. The sputter target is to the lower right.

3.2 Characterization

3.2.1 Thickness

The thickness measurements were carried out using a Dektak 150 stylus profilometer. To be able to use this method thickness step between the film and substrate is needed. This was achieved by using

a marker to draw a line on the substrates before the depositions. After the depositions this line was cleaned with acetone leaving an undeposited line on the substrate making it possible to measure the thickness.

SEM was used to measure the thickness of the samples from the FHR roll to roll sputter.

3.2.2 Sheet resistance

To measure the sheet resistance, two different devices were used. An Ossila T2001A3 and an AIT CMT-SR2000N. The Ossila is manually operated while the AIT is automatic. The results from both devices proved to be similar and hence no reference to which device was used will be mentioned in the results section.

3.2.3 Transmittance, reflectance and absorption coefficient

The transmittance and reflectance was measured using a Perkin Elmer lambda 900 spectrophotometer. A slit width of 1 nm was used and a measuring time of 0.4 s was used for each measured wavelength. The measurement interval used was 300-800 nm with 1 nm increments. The transmittance at 550 nm was used to calculate the absorption coefficient using the following equation:

$$\alpha = \frac{1}{d} \cdot ln(\frac{100}{\frac{100 \cdot T}{100 - R}}) \cdot 10^7 \tag{6}$$

where d is the thickness in nm and T/R the transmittance and reflectance at 550 nm [23]. This is essentially the same equation as equation 5 but fractions of incident light used instead of the intensity of light. 550 nm was used for these calculations as it is in the middle of the visible spectra. The factor at the end is added to get the desired unit of cm^{-1}

3.2.4 SEM

To acquire the SEM images, a Zeiss Merlin scanning electron microscope was used. All of the Von Ardenne and Lesker samples were viewed using the same acceleration voltage (5 kV) and due to the high resistance of some of the samples a conductive tape was used to prevent drift while acquiring the images.

The SEM images from the roll to roll sputter were acquired using an acceleration voltage of 2 keV.

4 Results

4.1 Von Ardenne

Figure 6 and 7 shows the behavior of the sheet resistance and resistivity respectively with changes in the oxygen flow used in the depositions from the first batch in the Von Ardenne sputter. The similarities between the two is due to all samples having similar thicknesses (Equation 1). Two depositions were done at 35 sccm as a big dip in sheet resistance was observed. This dip was observed in both cases although it was much bigger in the first deposition done.

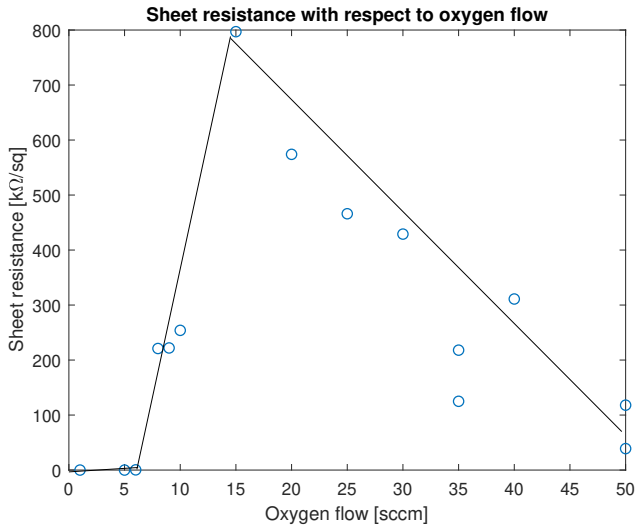

Figure 6: Sheet resistance as a function of oxygen flow for the samples from the Von Ardenne sputter. The deposition at 50 sccm with a lower sheet resistance was made using a very low argon flow. The solid lines indicate the overall trend and are guides for the eye only.

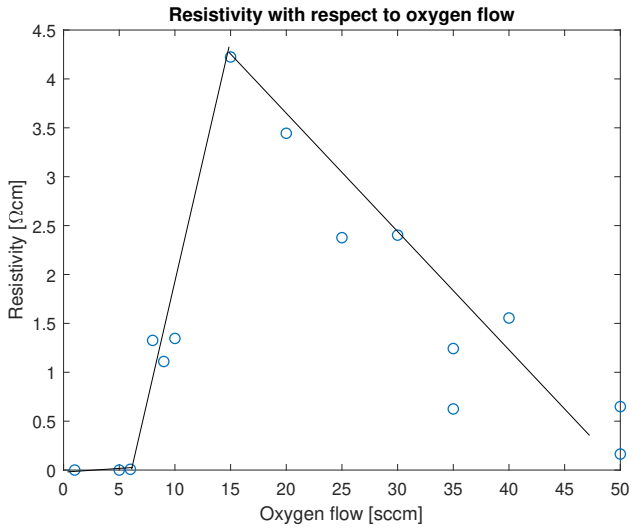

Figure 7: Resistivity as a function of oxygen flow for the samples from the Von Ardenne sputter. The deposition at 50 sccm that has lower resistivity was made using a very low argon flow. The solid lines indicate the overall trend and are guides for the eye only.

Figure 8 show how the absorption coefficient varies with changes in the oxygen flow used during the depositions from the Von Ardenne sputter. Figure 9 shows how the absorption coefficient is related to the resistivity. It can be seen that the absorption coefficient to a large extent, is independent of the oxygen flow despite large changes in resistivity.

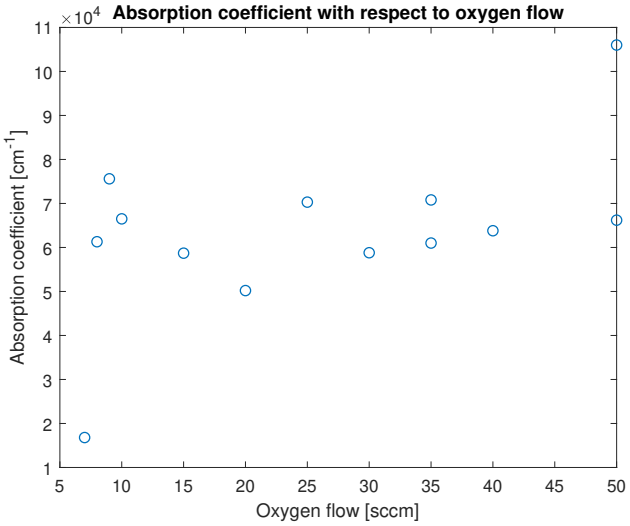

Figure 8: Absorption coefficient as a function of oxygen flow for the samples from the Von Ardenne sputter.

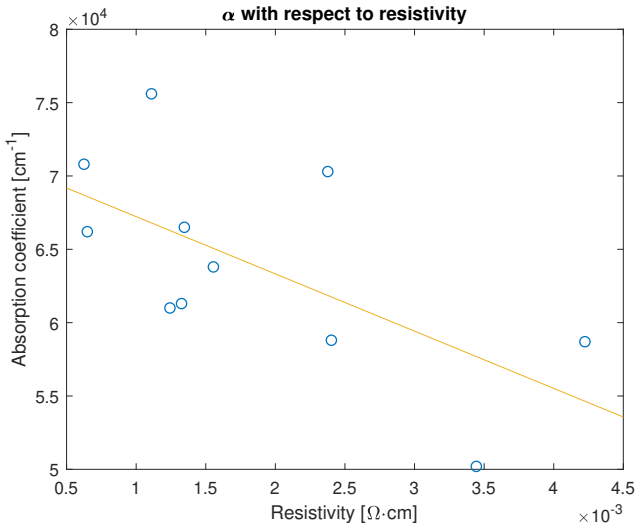

Figure 9: Absorption coefficient as a function of resistivity for the samples the Von Ardenne sputter. The yellow line is a linear fit.

Figures 10 - 12 shows how the discharge voltage, thickness and resistivity change around the transition from metal to oxide mode in the Von Ardenne sputter. This data is from the second batch of depositions done in the Von Ardenne. The sample deposited at 7 sccm is in the transition region while the samples below 7 sccm are in metal mode and the ones above in oxide mode.

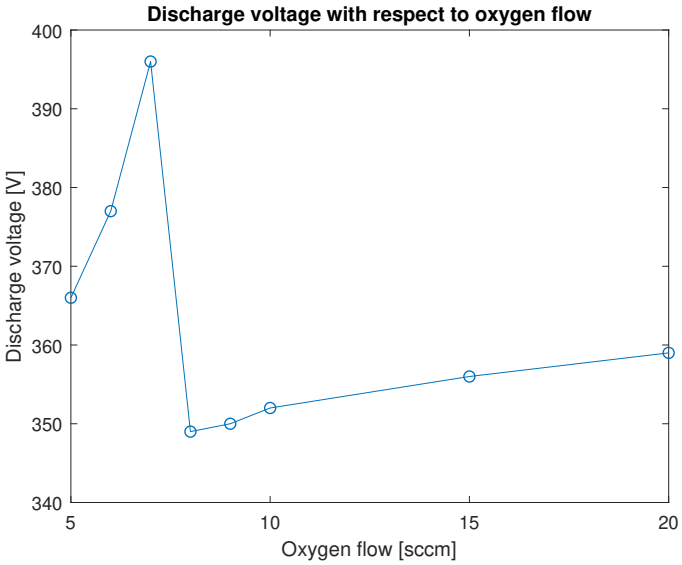

Figure 10: The discharge voltage as a function of oxygen flow in the area around the transition region in the Von Ardenne sputter. A clear transition can be seen at around 7 sccm.

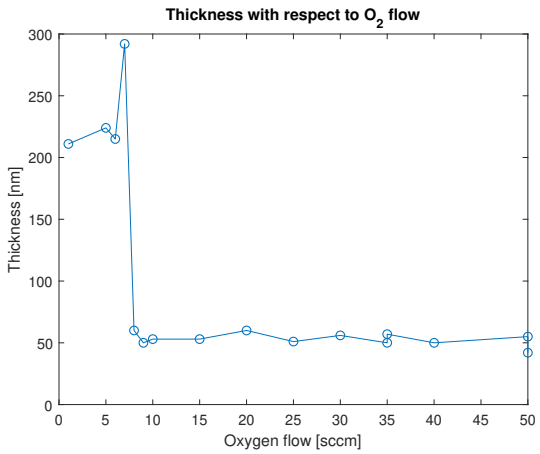

Figure 11: The thickness as a function of oxygen flow in the Von Ardenne sputter.

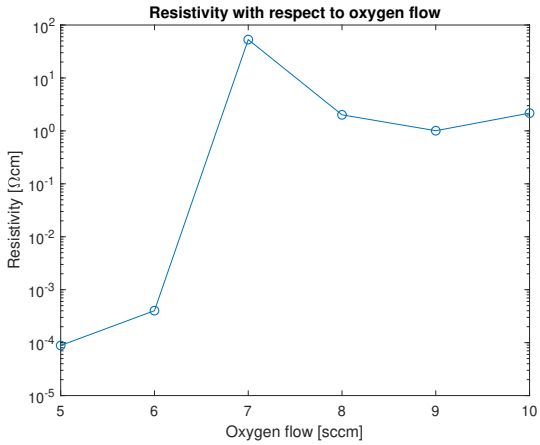

Figure 12: The resistivity as a function of oxygen flow in the Von Ardenne sputter.

Figure 13 shows the difference in absorption coefficient around the transition region in the Von Ardenne for the second batch of depositions with a clear drop at 7 sccm. Levels corresponding to annealed NiO and a literature value for NiO are added.

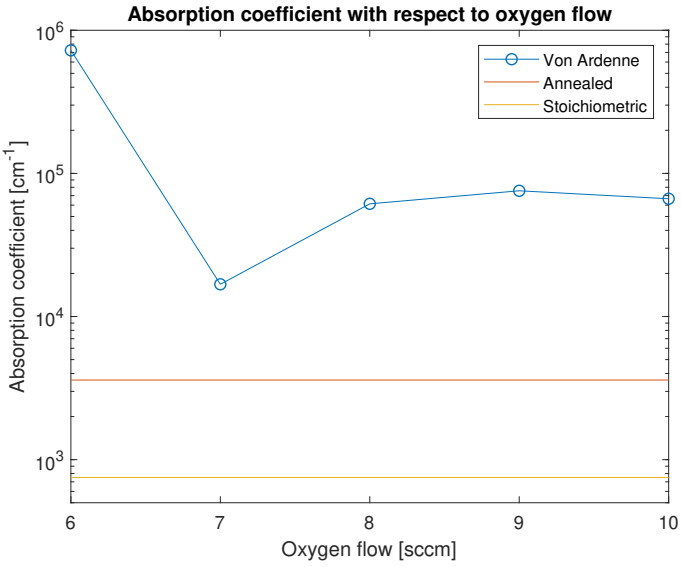

Figure 13: Absorption coefficient in the transition region in the Von Ardenne sputter. The orange line is an annealed film and the yellow line is stoichiometric NiO [11]. These lines were added for a comparison and were not deposited.

Figure 14 shows the transmittance for the first batch samples from the Von Ardenne. This data was used to calculate the absorption coefficient. Figure 15 shows how the absorption onset shifts for depositions done in the transition region compared to depositions done in oxide mode in the Von Ardenne sputter.

The wave-like shape in the transmittance curve for the 7 sccm sample is due to the film being thick enough to cause interference.

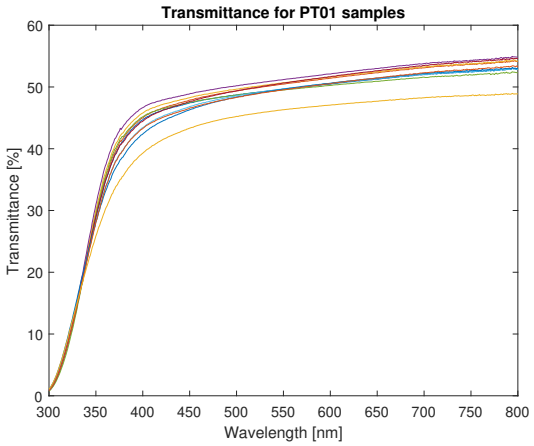

Figure 14: Transmittance for the samples from the Von Ardenne sputter deposited in oxide mode. This figure showcase the small spread in the transmittance between the samples.

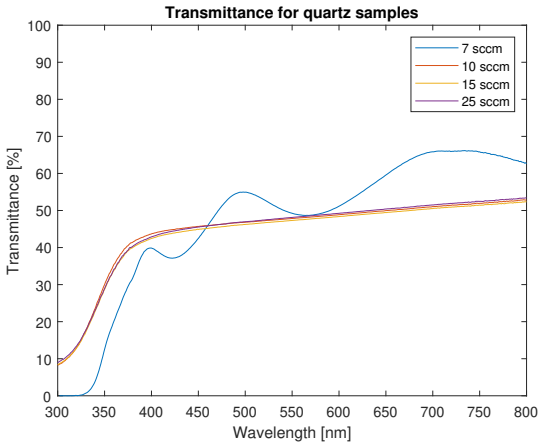

Figure 15: Transmittance for the quartz samples deposited in the Von Ardenne sputter. The difference between the transition region and oxide mode can clearly be seen.

Figure 16 shows the difference between a sample deposited in the transition region and one in oxide mode. The transmittance for both samples is roughly the same but interferance can be seen in the transition region sample on the left indicating that the film is much thicker than in oxide mode. As such the absorption coefficient is lower for the transition region sample than for the oxide mode sample.

Figure 16: Two samples deposited on quartz at two different oxygen flows in the Von Ardenne sputter. The left sample was deposited in the transition region at 7 sccm and the right in oxide mode at 15 sccm. The line that can be seen on both samples was used for thickness measurements.

Figure 17 is an SEM image depicting a cross section of the first 7 sccm sample deposited in the Von Ardenne sputter. The columnar structure that is typical for sputtered films can clearly be seen.

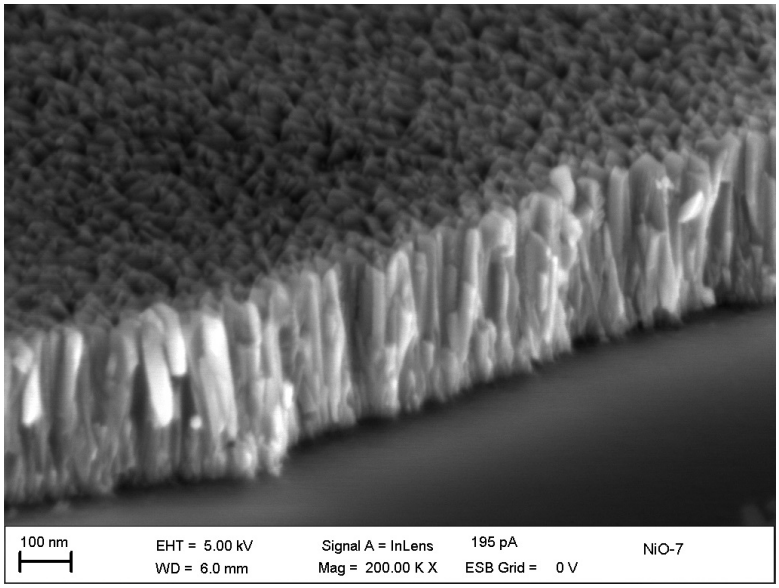

Figure 17: SEM image of film deposited in the transition region in the Von Ardenne.

4.2 Lesker

Figure 18 and table 5 show the transmittance and absorption coefficient for the narrow O_2-flow range second batch deposited in the Lesker sputter.

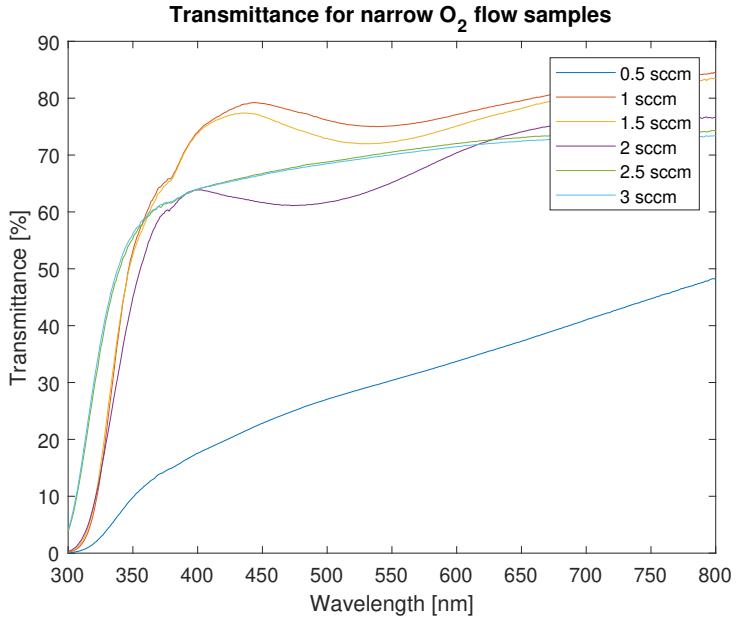

Figure 18: Transmittance for the Lesker samples deposited using small increments in the oxygen flow.

Table 5: The oxygen flow and corresponding thickness and absorption coefficient for the Lesker depositions done with a narrow range of oxygen flows.

Oxygen flow [sccm]	Thickness [nm]	Absorption coefficient [cm^{-1}]
0.5	193	$5.15 \cdot 10^4$
1	200	$4.62 \cdot 10^3$
1.5	187	$6.54 \cdot 10^3$
2	188	$1.41 \cdot 10^4$
2.5	27	$6.31 \cdot 10^4$
3	27	$6.81 \cdot 10^4$

Figure 19 shows the difference between samples deposited in the transition region and in the oxide region. The left and the middle samples were deposited in the transition region while the one on the right was deposited in oxide mode. The two samples from the transition region have a higher transmittance than the oxide mode sample despite being roughly seven times thicker which results in a lower absorption coefficient.

Figure 19: Three samples deposited on glass at three different oxygen flows in the Lesker sputter. The left sample was deposited in the transition region at 1 sccm, the middle sample in the transition region at 1.5 sccm and the right in oxide mode at 3 sccm. The thin line at the bottom of each sample was used to measure the thickness

Figure 20 is an SEM image of the first 1 sccm sample deposited in the Lesker sputter. This was the sample which had a substantially lower absorption coefficient than samples in oxide mode.

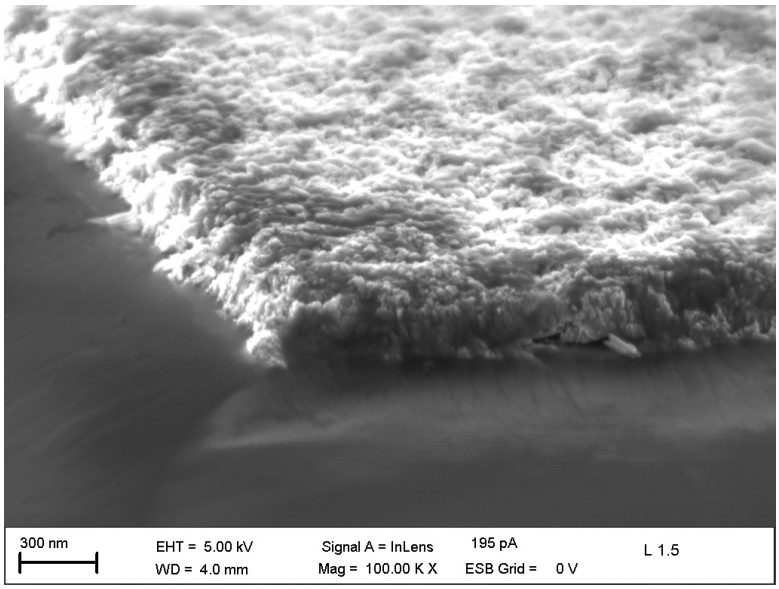

Figure 20: Film deposited in the semi-oxidized mode in the Lesker.

4.3 FHR roll-to-roll

Figure 21 and 22 show the transmittance and reflectance respectively for the low pressure deposition done in FHR sputter. There are clear differences between each oxygen flow used with the transmittance increasing with an increased oxygen flow. It is interesting to note that the samples with the highest transmittance also had the highest reflectance. The shift in the reflectance peaks are due to differences in the film thickness. Figure 23 and 24 show the same data but for the high pressure samples. The same behaviour as with the low pressure samples can be observed here. Figure 25 and 26 show the absorption spectra for the low and high pressure depositions respectively and what can be seen here in both cases is a decrease in absorptance as the oxygen flow increases.

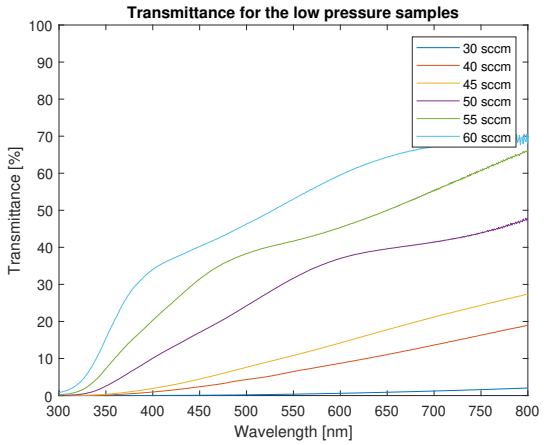

Figure 21: The transmittance for the low pressure deposition in the FHR roll to roll sputter

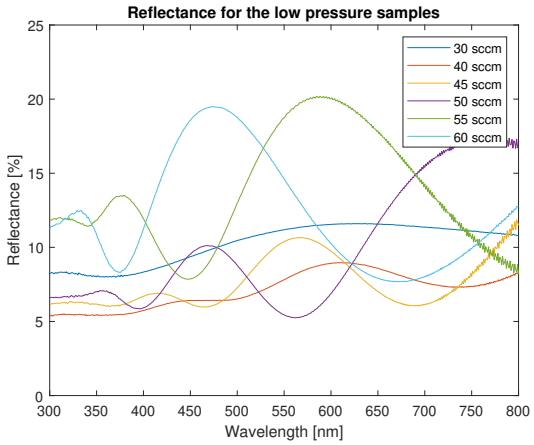

Figure 22: The reflectance for the low pressure deposition in the FHR roll to roll sputter.

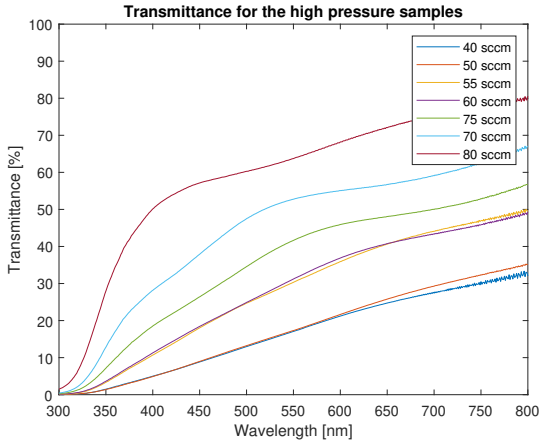

Figure 23: The transmittance for the high pressure deposition in the FHR roll to roll sputter for different oxygen flows.

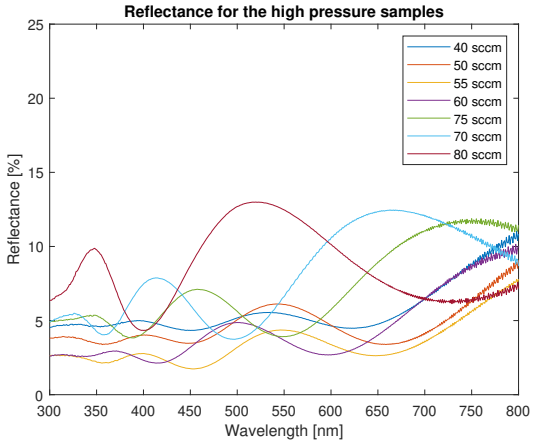

Figure 24: the reflectance for the high pressure deposition done in the FHR roll to roll sputter for different oxygen flows.

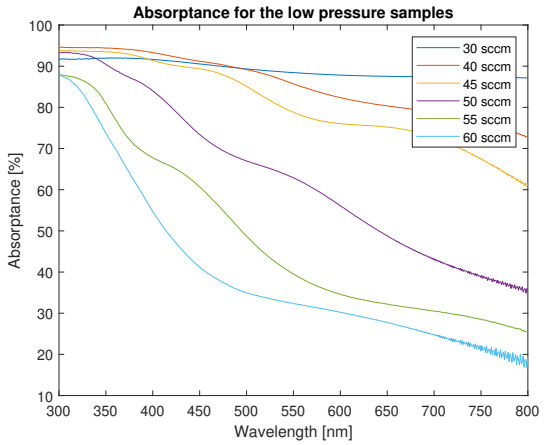

Figure 25: The absorptance for the low pressure deposition in the FHR roll to roll sputter for different oxygen flows.

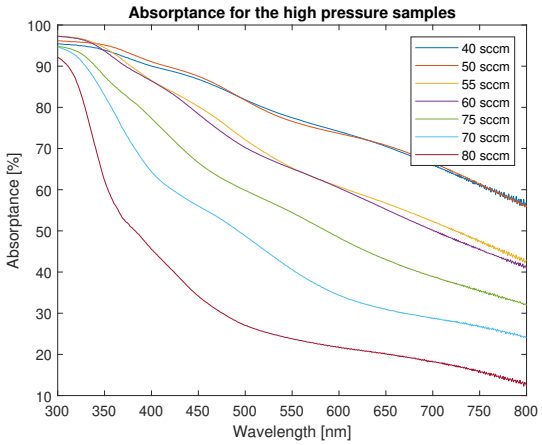

Figure 26: The absorptance for the high pressure deposition done in the FHR roll to roll sputter for different oxygen flows.

5 Discussion

More careful experiments showed that interesting NiO properties can be achieved close to the edge between metal mode and oxide mode, most noticeably a more transparent film than in oxide mode. Interestingly doing such a deposition results in a much higher deposition rate than in metal mode. The reason for the higher deposition rate as compared to the metal mode might be the difference in density between the pure nickel and NiO. Comparing the ratio between the densities of nickel and nickel oxide ($\frac{8.91}{6.67}$) and the ratio between the growth rate in the high deposition rate region and metal mode ($\frac{2.43}{1.87}$), almost the exact same number is achieved. As such they have the same mass deposition rate. More interesting is the comparison to the oxide mode of operation. Surprisingly, not only is the deposition rate higher but the films are also more transparent. The reason for this might be low reactivity between nickel and oxygen which leads to the target not getting poisoned while still allowing an oxide to form on the substrate. The first deposition done at 7 sccm in the Von Ardenne was the most transparent so far and had by far the highest resistivity which would make sense as the NiO should be close to stoichiometric.

The depositions done with the Lesker sputter using a narrow range of oxygen flows produced the films with by far the lowest absorption coefficient. Two of the films, 1 and 1.5 sccm had an absorption coefficient very close to that of annealed films. These films were also highly resistive with one being over the measurement range of equipment used and the other having the highest measured sheet resistance out of any films at 31 MΩ/□. With films deposited in the flow range of 0.5 to 2 sccm a much higher deposition rate was observed when compared to the depositions done at 2.5 and 3 sccm, indicating that they were deposited in or close to the edge of the transition region. Looking at table 5 it is clear that the depositions done at 1, 1.5 and 2 sccm were in transition region while the sample

deposited at 0.5 sccm likely is close to the edge of the transition region.

Apart from one, all samples that were deposited in the transition region were more transparent than any sample deposited in oxide mode. However it proved to be hard to make consistent depositions in the transition region with the Von Ardenne sputter resulting in poor reproducibility. The reason for this is uncertain but hysteresis effects might have an influence on the results here.

Figure 27 summarizes the absorption coefficients for the films deposited in this project and compares them to annealed films and stoichiometric NiO. The best films are very close to the annealed films showing that annealing can be avoided.

It is interesting to note that there are huge differences in the results from the two sputtering systems. In the Von Ardenne an increment of 1 sccm was the difference between the sputtering modes giving the transition window a width of at most 1 sccm. As such only one oxygen flow resulted in the depositions being done in the transition mode. However in the Lesker sputter the transition was a bit wider being a least 1.5 sccm.

There are several factors that can be contributing to the differences in the results between the two sputters. The main difference in the design of the two systems is where the gasses are introduced. In the Von Ardenne both the argon and oxygen are introduced in the same place while in the Lesker the argon is introduced around the target and oxygen is introduced around the substrate. This is likely a reason why the transition occurs at lower oxygen flows in the Lesker. Moreover, the different geometries likely contributed to the differences.

The window of oxygen flows that is in the transition region seems to be quite small. The increment in oxygen flow between the samples was 1 sccm in the Von Ardenne which was the difference between metal to transition and transition to oxide mode. The transition between the sputtering modes can be seen clearly in figure 10 - 13 where the optimum process point is around 7 sccm.

As the transition region is very narrow with a small increment in oxygen flow being the difference between being in the transition region and being in oxide mode, it is of interest to find an easy way to identify where this point is on different sputtering systems to find the desired process point. It was found that one way to do this is to monitor how the discharge voltage changes with oxygen flow. As can be seen in figure 10, the discharge voltage increases in metal and transition mode before dropping when reaching oxide mode. In this case the deposition done at an oxygen flow of 7 sccm is in the transition region. Hence by using an increasing amount of oxygen during the depositions, one can fairly easily find where the transition is by only monitoring the discharge voltage. This was utilized for depositions in the Lesker and FHR sputter. This also makes it possible to use a process control where the operating point is stabilized by an external controller [24].

The results from the first set of experiments in the Von Ardenne showed a clear increase in sheet resistance once oxide mode was reached and continued to increase with an increased oxygen flow up to a point after which it starts to decrease, as can be seen in figure 6. This deviates somewhat from the behavior that could be expected namely a sharp increase in sheet resistance once oxide mode is reached followed by a steady decrease with an increased oxygen flow [14, 16]. The films however turned out to be fairly absorbing with the absorption not changing much with oxygen flow. This behavior was observed in both the Von Ardenne and Lesker sputter with one anomaly for each machine. In the case with the Von Ardenne sputter a big dip in sheet resistance was observed at an oxygen flow of 35 sccm as can be seen in figure 6. The reason for this is uncertain. The samples from the Von Ardenne which were deposited in oxide mode all had a thickness of 50 ± 5 nm.

For the Lesker samples, the ones using the same sputtering time and different oxygen flows show this expected behavior although only a few different oxygen flows were used which makes it hard to make comparisons with the Von Ardenne samples. The sample that had a sputtering time of one hour with an oxygen flow of 5 sccm ended up with a much higher sheet resistance than what could be expected. The reason for this is uncertain.

As the oxygen flow increases more nickel vacancies should be introduced in the material. These vacancies should scatter and absorb light lowering the transmittance of the films. As previously mentioned these vacancies are also responsible for the conduction in NiO so what could be expected is a more absorbing and less resistive film as the oxygen flow is increased. As can be seen in figure 7, the resistance decreases as expected although the change is not all that big. A factor of four differs between the most and least resistive samples, not taking into account the samples deposited at 1 and 5 sccm as they were metallic.
Although the absorption coefficient does not change much with the oxygen flow as can be seen in figure 8, it is worth noting that it is two orders of magnitude higher than for stoichiometric NiO.

Due to the resistivity and absorption coefficient theoretically having an expected behavior with respect to oxygen flow, plotting them against each other is interesting. Here a decrease in absorption coefficient is expected with an increased resistivity. As can be seen in figure 9, this behavior can somewhat be seen in the Von Ardenne samples as shown by the linear fit, although correlation seems to be weak. However it is worth noting that the films are absorbing and much more so than annealed films.

The results from the Lesker samples are inconclusive as depositions were only done around the transition region so more depositions would need to be done to sort out whether this behaviour is present.

As can be seen in figure 14 the absorption onset is fairly similar for all samples at around 370 nm and the transmittance after the onset overlaps completely for all samples. NiO has a band gap around 4 eV which corresponds to roughly 310 nm. This does not correspond to the observed data in figure 14 and hence it is most likely the glass substrate that is responsible for the absorption. Hence to measure the band gap, another substrate material would have to be used.

Depositions done on quartz showed similar results regarding transmittance as the ones done on glass showing that the band gap of the NiO is close to where the glass starts to absorb. However it is interesting that all the depositions done in oxide mode had a pretty much overlapping transmittance curve, indicating that the band gap does not change with the oxygen flow. The deposition done at 7 sccm in the transition region however started to absorb at higher wavelenghts as can be seen in figure 15 and hence it has a lower band gap.

Looking at the transmittance curves in figure 18 it is interesting to see that the absorption onset is overlapping for the samples deposited at 1, 1.5 and 2 sccm. As previously mentioned all the depositions done in oxide mode had an overlapping onset indicating that they have the same band gap and that a shift in band gap was observed when in the transition region. Here it seems that different oxygen flows in the transition region does not affect the band gap. The reason for the difference in band gap between the NiO deposited in transition and oxide mode is uncertain.

When looking at films sputtered in the same mode from Von Ardenne and Lesker, a clear difference in microstructure was observed. The samples from figure 17 and 20 were deposited in the transition region and should therefore be comparable. There may be a few reasons as to why this difference is observed. Different types sputtering were used which may have an effect here. The main reason however is most likely the difference in design between the two systems. The lower power used and the larger target to substrate distance in the Lesker leads to lower energy of the species arriving at the substrate as compared to the Von Ardenne and this is likely why the Von Ardenne film is smoother. It is worth mentioning that the target to substrate distance is short enough in the Von Ardenne to allow the plasma to get close to the substrate further increasing the energy of the species reaching it.

There was a clear visual difference between the two depositions done in the FHR. The one done with a lower argon flow and pressure had clearly visible transitions between the sections with different oxygen flows. The deposition done at a higher pressure only had one visible transition from 40-50 sccm while the rest of the foil looked pretty much identical with a dark brown coloration. The foil in both of the depositions wrinkled, most likely due to heat because of the high power used and the fact that the polymer substrate was insulating. The visual appearance changed for the high pressure samples in the days between the cutting of the foil and the transmittance and reflectance measurements with the different parts having a more transparent look rather than dark brown. The reason for this is uncertain.

The transmittance and reflectance measurements yielded some interesting results. Most noticeable is that an interference pattern is observed in the reflectance measurements for both the high and low pressure depositions but not in the transmittance measurements for either of the depositions. The reason here might be related to the polymer substrate but this is unconfirmed. The results from both depositions were very similar with an increase in transmittance as the oxygen flow increased. It is however worth noting that in the high pressure depositions there were two overlapping transmittance curves, the deposition done at 40 and 50 sccm as well as at 55 and 60 sccm. This overlap is not present in the reflectance measurements.

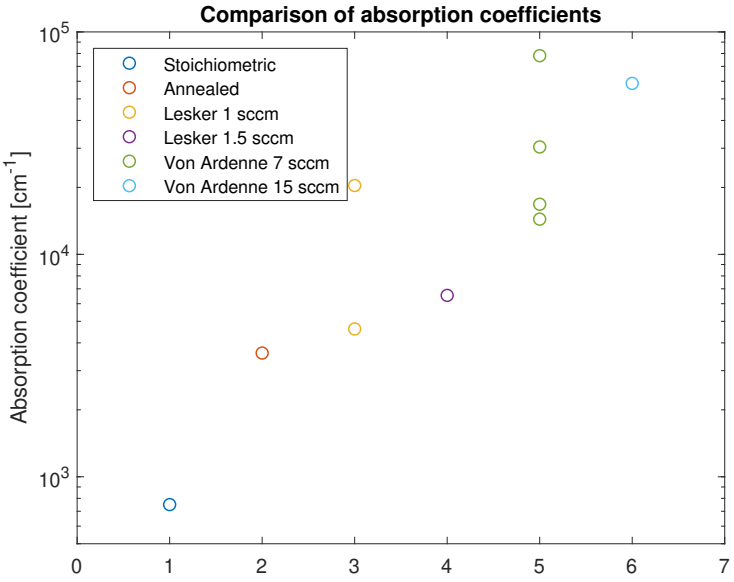

Figure 27: Comparison between the absorption coefficient of different oxygen flows and sputters with annealed and stoichiometric NiO. All depositions in this figure were done in the transition region apart from the 15 sccm sample from the Von Ardenne which was deposited in oxide mode.

6 Conclusions and future work

A region when transparent and highly resistive NiO is deposited was found close to the edge betweeen metal and oxide mode. The depositions made in this region have a very high deposition rate, even more so than in metal mode and a lot higher than in oxide mode. This is a surprising finding that is likely connected to the sputtering target remaining unpoisoned due to low reactivity between nickel and oxygen. The process characteristics may be important and will need to be investigated to sort out why this region exists and why the deposition rate increases. X-ray photoelectron spectroscopy would

need to be used to evaluate the composition of the material sputtered in the transition region.

The developed process shows promise for solar cell and electrochromic applications. Possibly leading to more efficient tandem solar cells as well as improved smart windows which can make buildings more energy efficient.

Acknowledgments

First of all I would like to thank my supervisor Tomas Kubart for the chance to do this project. Your input and guidance throughout the journey has been immensely valuable and pushed me forwards when I was at a loss.

I would like to thank Tobias Törndahl for reviewing the project and providing valuable input throughout the course of the project.

A big thank you goes to MyFab who let me access their lab at Ångström and use their equipment.

Thank you to Tomas Nyberg who provided me with support and instructions on how to run most of the experimental equipment. I would also like to thank him for providing a fun atmosphere whenever he was around.

Thank you to Gunnar Niklasson who with his vast knowledge about NiO, provided me with valuable discussions and information about the material and its properties.

A big thank you to Daniel Fernandes for proofreading the report and providing me with input on how to improve it.

Thank you to all my friends and my family for supporting me during this project.

And finally I would like to thank my girlfriend Kellie Sellin Edland who has supported me and put up with my antics throughout the course of the project.

References

[1] Milton Ohring. *Materials science of thin films*. Elsevier, 2001.

[2] Peter M Martin. *Handbook of deposition technologies for films and coatings: science, applications and technology*. William Andrew, 2009.

[3] A Belkind, A Freilich, J Lopez, Z Zhao, W Zhu, and K Becker. Characterization of pulsed dc magnetron sputtering plasmas. *New Journal of Physics*, 7(1):90, 2005.

[4] B Window and F Sharples. Magnetron sputtering sources for ferromagnetic material. *Journal of Vacuum Science & Technology A: Vacuum, Surfaces, and Films*, 3(1):10–13, 1985.

[5] Matt Hughes. What is dc sputtering? *Semicore Equipment Inc*, url:http://www.semicore.com/news/94–what–is–dc–sputtering, Written 2016-11-26. Taken on 2020-9-21.

[6] Jun-Yuan Jeng, Kuo-Cheng Chen, Tsung-Yu Chiang, Pei-Ying Lin, Tzung-Da Tsai, Yun-Chorng Chang, Tzung-Fang Guo, Peter Chen, Ten-Chin Wen, and Yao-Jane Hsu. Nickel oxide electrode interlayer in ch3nh3pbi3 perovskite/pcbm planar-heterojunction hybrid solar cells. *Advanced materials*, 26(24):4107–4113, 2014.

[7] Zhenwei Wang, Pradipta K Nayak, Jesus A Caraveo-Frescas, and Husam N Alshareef. Recent developments in p-type oxide semiconductor materials and devices. *Advanced Materials*, 28(20):3831–3892, 2016.

[8] Gunnar A Niklasson and Claes G Granqvist. Electrochromics for smart windows: thin films of tungsten oxide and nickel oxide, and devices based on these. *Journal of Materials Chemistry*, 17(2):127–156, 2007.

[9] E Avendano, A Azens, J Isidorsson, R Karmhag, GA Niklasson, and CG Granqvist. Optimized nickel-oxide-based electrochromic thin films. *Solid State Ionics*, 165(1-4):169–173, 2003.

[10] Esteban Damián Avendaño Soto. *Electrochromism in nickel-based oxides: coloration mechanisms and optimization of sputter-deposited thin films*. PhD thesis, Acta Universitatis Upsaliensis, 2004.

[11] R Newman and RM Chrenko. Optical properties of nickel oxide. *Physical Review*, 114(6):1507, 1959.

[12] Jorge Osorio-Guillén, Stephan Lany, and Alex Zunger. Nonstoichiometry and hole doping in nio. In *AIP Conference Proceedings*, volume 1199, pages 128–129. American Institute of Physics, 2010.

[13] Wei-Luen Jang, Yang-Ming Lu, Weng-Sing Hwang, Tung-Li Hsiung, and H Paul Wang. Point defects in sputtered nio films. *Applied Physics Letters*, 94(6):062103, 2009.

[14] H Sato, T Minami, S Takata, and T Yamada. Transparent conducting p-type nio thin films prepared by magnetron sputtering. *Thin solid films*, 236(1-2):27–31, 1993.

[15] Yong Hun Kwon, Sung Hyun Chun, Jae-Hee Han, and Hyung Koun Cho. Correlation between electrical properties and point defects in nio thin films. *Metals and Materials International*, 18(6):1003–1007, 2012.

[16] Julien Keraudy, Brice Delfour-Peyrethon, Axel Ferrec, Javier Garcia Molleja, Mireille Richard-Plouet, Christophe Payen, Jonathan Hamon, Benoît Corraze, Antoine Goullet, and Pierre-Yves Jouan. Process-and optoelectronic-control of niox thin films deposited by reactive high power impulse magnetron sputtering. *Journal of Applied Physics*, 121(17):171916, 2017.

[17] Kazuki Yoshimura, Takeshi Miki, and Sakae Tanemura. Nickel oxide electrochromic thin films prepared by reactive dc magnetron sputtering. *Japanese journal of applied physics*, 34(5R):2440, 1995.

[18] Walter Johnson and Chuck Yarling. Sheet resistance and the four point probe. In *Characterization in Silicon Processing*, pages 208–216. Elsevier, 1993.

[19] Sheet resistance theory. `https://www.ossila.com/pages/sheet-resistance-theory`. Accessed: 2020-09-14.

[20] David S Ginley, Hideo Hosono, David C Paine, et al. *Handbook of Transparent Conductors*. Number 978-1-4419-1638-9. springer, 1st edition, 2010.

[21] Mark Fox. Optical properties of solids, 2002.

[22] Yang Leng. *Materials characterization: introduction to microscopic and spectroscopic methods*. John Wiley & Sons, 2009.

[23] C Guillén and J Herrero. Transparent and p-type conductive nixo: V thin films obtained by reactive dc sputtering at room temperature. *Materials Research Express*, 6(9):096410, 2019.

[24] William D Sproul, David J Christie, and Dan C Carter. Control of reactive sputtering processes. *Thin solid films*, 491(1-2):1–17, 2005.

Appendix

Figure 28 and 29 were used to identify the transition region for the two depositions done in the FHR roll to roll machine and the oxygen flows used were based on these graphs. Figure 30 shows the shift in transition region due to the pressure differences.

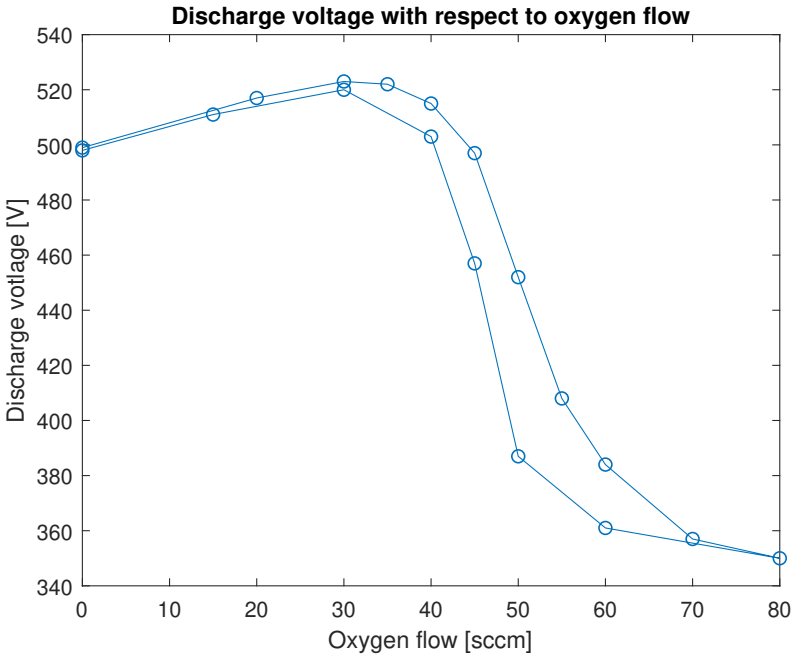

Figure 28: Discharge voltage as a function of oxygen flow for the low pressure depositions done in the FHR roll to roll sputter.

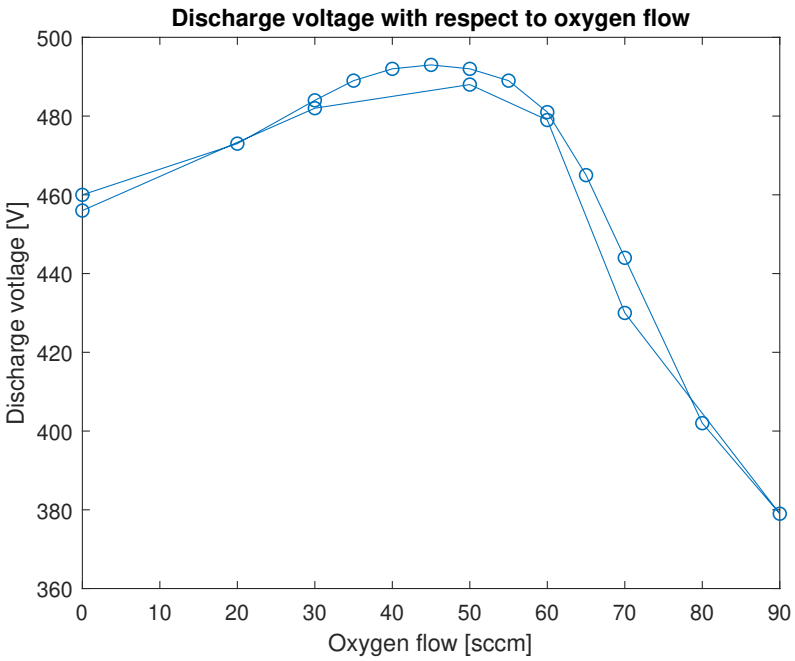

Figure 29: Discharge voltage as a function of oxygen flow for the high pressure depositions done in the FHR roll to roll sputter.

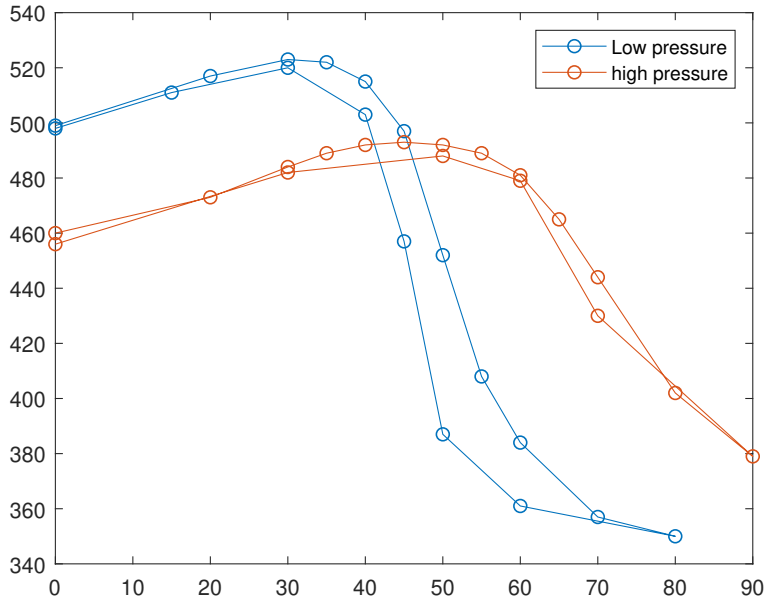

Figure 30: Comparison of the discharge voltages with the two different pressures used in the FHR

Figure 31 shows the optical transmittance reflectance and absorptance for the glass substrates. This was used to determine that it was the glass and NiO that was absorbing close to UV wavelengths.

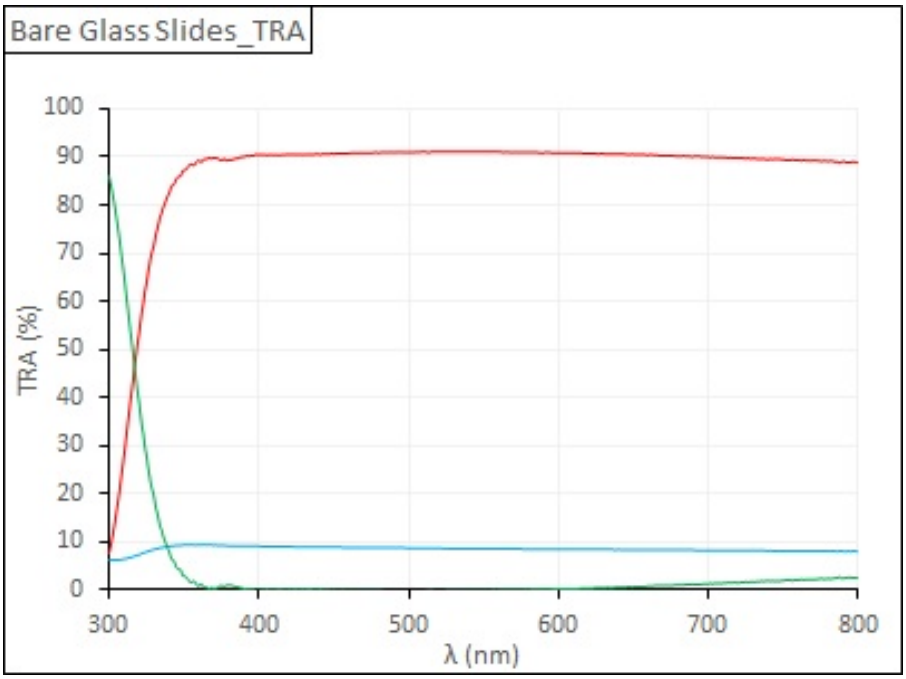

Figure 31: Transmittance, reflectance and absorptance for the glass substrates used